Dynamic Nature of Cleavage Bodies and Their Spatial Relationship to DDX1 Bodies, Cajal Bodies, and Gems

Lei Li, Ken Roy, Sachin Katyal, Xuejun Sun, Stacey Bléoo, and Roseline Godbout

Department of Oncology, University of Alberta, Cross Cancer Institute, Edmonton, Alberta T6G 1Z2, Canada

DDX1 bodies, cleavage bodies, Cajal bodies (CBs), and gems are nuclear suborganelles that contain factors involved in RNA transcription and/or processing. Although all four nuclear bodies can exist as distinct entities, they often colocalize or overlap with each other. To better understand the relationship between these four nuclear bodies, we examined their spatial distribution as a function of the cell cycle. Here, we report that whereas DDX1 bodies, CBs and gems are present throughout interphase, CPSF-100-containing cleavage bodies are predominantly found during S and G2 phases, whereas CstF-64-containing cleavage bodies are primarily observed during S phase. All four nuclear bodies associate with each other during S phase, with cleavage bodies colocalizing with DDX1 bodies, and cleavage bodies/DDX1 bodies residing adjacent to gems and CBs. Although inhibitors of RNA transcription had no effect on DDX1 bodies or cleavage bodies, inhibitors of DNA replication resulted in loss of CstF-64-containing cleavage bodies. A striking effect on nuclear structures was observed with latrunculin B, an inhibitor of actin polymerization, resulting in the formation of needlelike nuclear spicules made up of CstF-64, CPSF-100, RNA, and RNA polymerase II. Our results suggest that cleavage body components are highly dynamic in nature.

INTRODUCTION

The DEAD box protein DDX1 is a putative RNA unwinding protein that has been associated with RNA processing as well as RNA transport (Bleoo *et al.,* 2001; Kanai *et al.,* 2004). DDX1 has a widespread punctate distribution pattern in the nucleus and is also found in discrete nuclear bodies with an estimated diameter of ~0.5 μm (Bleoo *et al.,* 2001). These DDX1 bodies frequently colocalize with cleavage bodies. Cleavage bodies were first identified by immunofluorescence labeling using antibodies against cleavage stimulation factor CstF-64 and the cleavage and polyadenylation specificity factor CPSF-100 (Schul *et al.,* 1996). Transcription factors TFIIE and TFIIF have also been found to colocalize with cleavage bodies (Gall, 2000). Cleavage bodies have diameters of 0.3–1 μm and range in number from 1 to 4 per nucleus (Schul *et al.,* 1996). Based on FRET analysis and coimmunoprecipitation experiments, DDX1 and CstF-64 proteins are in close proximity to each other and can reside in the same complex (Bleoo *et al.,* 2001).

Cleavage bodies frequently associate with Cajal bodies (CBs, also known as coiled bodies) in the nucleus (Schul *et al.,* 1996, 1999). CBs have diameters ranging from 0.2 to 1.0 μm, and number from 1 to 10 per nucleus. The Sm epitope, shared by small nuclear ribonucleoproteins (snRNPs), was the first molecular component identified in CBs (Eliceiri and Ryerse, 1984; Fakan *et al.,* 1984). Subsequent analyses showed that p80-coilin protein is also highly enriched in CBs

(Andrade *et al.,* 1991; Raska *et al.,* 1991). In addition to Sm proteins and p80-coilin, CBs contain a large variety of proteins including RNA polymerases, transcriptional factors, and nucleolar constituents. Based on its protein content, CBs have been proposed to play roles in snRNP and small nucleolar ribonucleoprotein (snoRNP) biogenesis, posttranscriptional modification of spliceosomal snRNAs, assembly site for the transcription machinery, and pre-rRNA processing (reviewed in Matera, 1999; Gall, 2000; Ogg and Lamond, 2002; Cioce and Lamond, 2005). CBs are closely associated with histone gene clusters in both amphibians and mammalian cells (Gall *et al.,* 1981; Callan *et al.,* 1991; Frey and Matera, 1995; Schul *et al.,* 1999). Consistent with a role in histone gene transcription, CBs contain U7 snRNP, which is required for processing the 3′-end of histone pre-mRNA (Wu and Gall, 1993; Frey and Matera, 1995; Wu *et al.,* 1996). Cyclin E and CDK2 have been shown to localize to CBs at the G1/S boundary of the cell cycle, when cyclin E is first expressed (Liu *et al.,* 2000). The cyclin E/CDK2 interacting protein p220/NPAT, also found in CBs, has been proposed to link cyclin E/CDK2 kinase activity to histone gene transcription (Ma *et al.,* 2000).

Gems are nuclear structures that are indistinguishable from CBs in most cell lines and adult tissues (Matera and Frey, 1998; Young *et al.,* 2000). Work carried out in Hela PV and fetal tissues demonstrates that gems can also reside adjacent to or exist separately from CBs (Liu and Dreyfuss, 1996; Young *et al.,* 2001; Hebert *et al.,* 2002). Gems contain the survival motor neuron (SMN) protein encoded by the *SMN1* gene, which is frequently mutated or deleted in spinal muscular atrophy (SMA; Lefebvre *et al.,* 1995). SMN forms a complex with Gemins 2–7 and interacts with Sm, Sm-like proteins, RNA helicase A, and hnRNP R, Q, and U (reviewed in Gubitz *et al.,* 2004). The SMN-protein complex plays a critical role in snRNP biogenesis (Pellizzoni *et al.,* 2002; Yong *et al.,* 2002) and has been implicated in the assembly of snoRNP particles (Pellizzoni *et al.,* 2001a) and
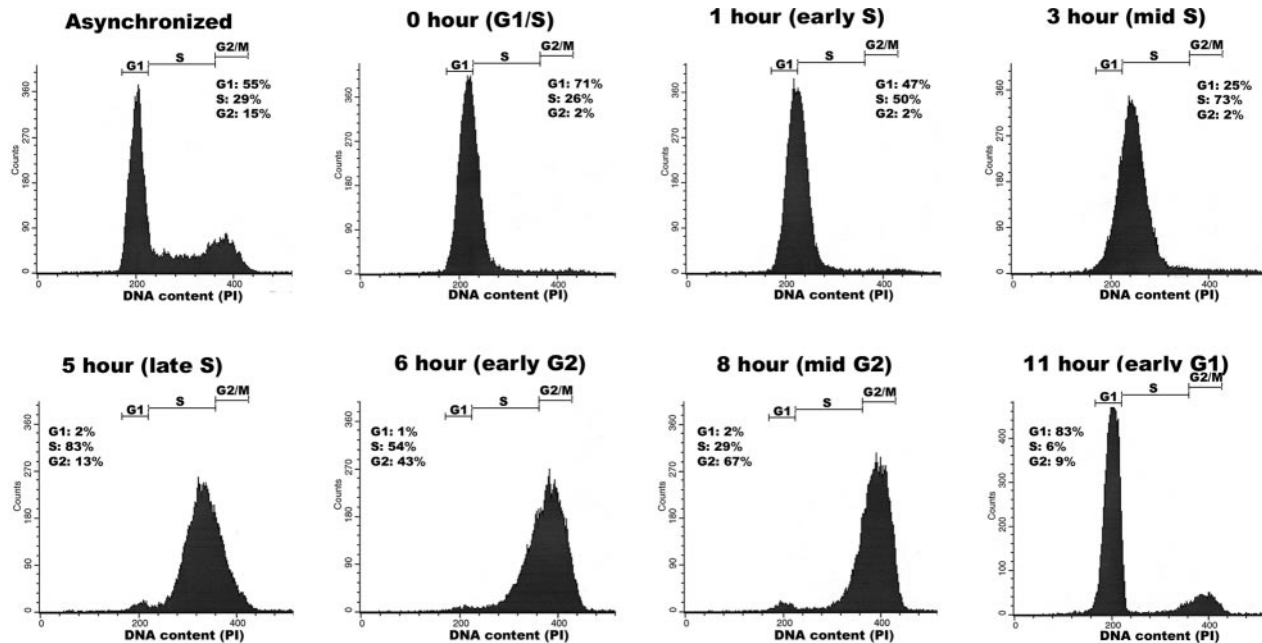
Figure 1. Flow cytometry analysis of synchronized HeLa cells. Cells were synchronized using the double thymidine block method. Cells released from arrest were collected at the indicated time points and analyzed by flow cytometry. For each time point, the percentage of cells in G1, S, and G2 phases are shown in the insets.

the pol II transcription/processing machinery (Pellizzoni *et al.*, 2001b). Consistent with the close association observed between gems and CBs, SMN interacts directly with p80-coilin and absence of p80-coilin prevents recruitment of SMN to CBs (Hebert *et al.*, 2001; Tucker *et al.*, 2001). The symmetrical dimethylarginines of p80-coilin regulate its interaction with SMN and determine whether SMN will localize to CBs (Hebert *et al.*, 2002).

The close association between DDX1 bodies, cleavage bodies, CBs, and gems suggests that they may play an interactive role in the cell, perhaps by providing factors or preassembled complexes required for RNA transcription and/or processing. To more closely define the relationship between these four nuclear bodies, we carried out a series of triple-labeling experiments using antibodies to DDX1 (DDX1 bodies), SMN (gems), CstF-64/CPSF-100 (cleavage bodies), and Sm (CBs) at different stages of the cell cycle. Nuclear bodies were visualized by confocal microscopy and were three-dimensionally reconstructed to reveal the location of each nuclear body with respect to the others. Here, we report specific patterns of associations between these four nuclear bodies depending on the stage of the cell cycle. We also demonstrate that inhibitors of RNA transcription, DNA replication, and actin polymerization specifically affect subsets of nuclear bodies and/or their protein composition. Our data support a role for actin polymerization in the movement or distribution of CstF-64 and CPSF-100 within the nucleus.

MATERIALS AND METHODS

Cell Synchronization, Flow Cytometry, and Drug Treatment

Two types of HeLa cells were used: HeLa (ATCC, Rockville, MD) and HeLa PV obtained from Dr. Gideon Dreyfuss (University of Pennsylvania School of Medicine, Philadelphia, PA). HeLa cells were grown on glass coverslips in DMEM supplemented with 10% fetal calf serum, 100 U/ml penicillin, and 100

μg/ml streptomycin. HeLa cells were synchronized using the double thymidine block method modified from Pederson and Robbins (1971); i.e., cells were exposed to 2.5 mM thymidine for 12 h, and the thymidine was removed for 12 h, after which time thymidine was added for an additional 12 h. To determine number of cells at different stages of the cell cycle, cells were harvested at 0 (immediately after removal of the second thymidine block), 1, 3, 4, 5, 6, 8, 10, 11, and 12 h. In the case of HeLa PV, cells were harvested at 3, 6, and 11 h. Propidium iodide-stained cells were gated to remove cell debris and aggregates and analyzed by flow cytometry (FACSort using Cell Quest version 3.2.1, BD Biosciences, San Jose, CA). Based on the profiles obtained from this analysis, we have chosen the following time points: 1, 3, 5, 6, 8, and 11 h, to represent early S (50% of cells in S), mid-S (73% of cells in S), late S (83% of cells in S), early G2 (43% of cells in G2), mid-G2 (67% of cells in G2), and early G1 phase (83% of cells in G1), respectively (Figure 1). Note that cells in mitosis were not analyzed because previous studies have shown that nuclear bodies disappear during this stage of the cell cycle (Andrade *et al.*, 1993; Schul *et al.*, 1996; Bleoo *et al.*, 2001).

The procedure for GM38 (normal human fibroblasts) synchronization was as described above except that the cells were cultured in the presence of thymidine for 16 h instead of 12 h (with a 12-h interval between the two thymidine blocks). To study cells in S phase, cells were immunostained 3 h after release from the second thymidine block. The percentage of GM38 cells arrested in S phase was examined by adding 5-bromo-deoxyuridine (BrdU, Sigma, St. Louis, MO) to a final concentration of 200 μM 30 min before immunostaining.

Cells were treated with the following drugs: 6 μg/ml actinomycin D (Sigma) for 1 h, 50 μg/ml α-amanitin (Sigma) for 4 h, 10 μg/ml aphidicolin (Sigma) for 1 h, 4 mM hydroxyurea (Sigma) for 1 h, 5 μM latrunculin B (Calbiochem, San Diego, CA) for 40 min, and 20 μM cytochalasin D (Sigma) for 40 min. With the exception of α-amanitin, cells were released from the second thymidine block for 2.5 h before adding the drug. In the case of α-amanitin, cells were treated with the drug immediately after release from the second thymidine block. To monitor the efficiency of actinomycin D treatment, 5-fluorouridine (5-FU, Sigma) was added to a final concentration of 1.3 mM 30 min after addition of actinomycin D. To pulse-label cells with 5-FU, cells were incubated in 1.3 mM 5-FU for 10 min followed by growth in medium without 5-FU for 40 min. For the experiments where both actinomycin D and latrunculin B were used, cells were first treated with 6 μg/ml actinomycin D for 60 min and then subjected to 5 μM latrunculin B for 40 min. To monitor the efficiency of aphidicolin treatment, BrdU was added to a final concentration of 200 μM 30 min after addition of aphidicolin.

Immunofluorescence Labeling

Cells adhering to coverslips were fixed in 1% paraformaldehyde in phosphate-buffered saline (PBS) for 10 min and permeabilized for 5 min in 0.5%

Triton X-100 in PBS. A higher percentage of paraformaldehyde (3%) was used for the latrunculin B and cytochalasin D experiments in order to maximize retention of cells on coverslips. Cells were immunostained with rabbit anti-DDX1 antibody (batch 2923) at a 1:1000 dilution (Bleoo *et al.,* 2001), goat anti-CstF-64 antibody at a 1:100 dilution (Santa Cruz Biotechnology, Santa Cruz, CA), mouse anti-CstF-64 at a 1:1000 dilution (gift from Dr. James Manley, Columbia University), goat anti-CPSF2 (CPSF-100) at a 1:100 dilution (Santa Cruz Biotechnology), mouse anti-SMN antibody at a 1:1000 dilution (BD Biosciences), goat anti-SMN (N-19) antibody at a 1:100 dilution (Santa Cruz Biotechnology), mouse anti-RNA polymerase II antibody (H5) at a 1:100 dilution (Bregman *et al.,* 1995), rabbit anti-hnRNP K at a 1:100 dilution (gift from Dr. Pradip Raychaudhuri, University of Illinois at Chicago), and mouse anti-Sm monoclonal antibody (mAb) Y12 at a 1:3000 dilution (gift from Dr. Joan Steitz, Yale University). The Y12 antibody recognizes multiple Sm antigens of the snRNPs within CBs (Lerner *et al.,* 1981). Because many of our experiments involved triple-labeling, we frequently had to use the mouse Y12 antibody rather than the more commonly used rabbit p80-coilin antibody to detect CBs. To ensure that these two antibodies are equally efficient at recognizing CBs, we examined their colocalization within CBs by coimmunostaining HeLa cells (ATCC) with mouse anti-Sm antibody and rabbit anti-p80 coilin antibody (gift from Dr. Edward Chan, University of Florida at Gainesville). Examination of more than 50 cells revealed >95% colocalization in CBs, consistent with previous reports indicating that both p80-coilin and Sm are found within CBs (reviewed in Gall, 2000) and that the Y12 antibody recognizes both Sm and p80-coilin proteins (Hebert *et al.,* 2002).

In some experiments, we monitored either BrdU incorporation into DNA or 5-FU incorporation into RNA using anti-BrdU antibodies. Anti-BrdU antibody (Roche, Laval, Quebec, Canada) was used at a 1:50 dilution to monitor DNA synthesis. To detect 5-FU incorporation, a 1:200 dilution of anti-BrdU antibody (Sigma) was used (anti-BrdU antibody also recognizes 5-FU; Boisvert *et al.,* 2000). The mouse mAb to actin (clone C4; ICN Biomedicals, Costa Mesa, CA), which detects nuclear actin (Gedge *et al.,* 2005), was used at a 1:100 dilution. Secondary antibodies included Alexa 488 donkey anti-mouse, Alexa 488 donkey anti-rabbit, Alexa 555 donkey anti-goat, Alexa 555 goat anti-mouse (all from Molecular Probes, Eugene, OR), and Cy5 donkey anti-rabbit (Jackson ImmunoResearch Laboratories, West Grove, PA). All secondary antibodies were used at a 1:200 dilution. Coverslips were mounted onto slides with glycerol containing 1 mg/ml ρ-phenylenediamine and 1 μg/ml 4',6-diamidino-2-phenylindole (DAPI).

For triple-staining with anti-DDX1, anti-CstF-64, and anti-BrdU antibodies (see Figures 8 and 9), cells were fixed in 1% paraformaldehyde and incubated with anti-DDX1 and anti-CstF-64 antibodies, followed by secondary antibody staining. Cells were then washed with PBS, fixed in 4% paraformaldehyde, treated with 2 N HCl for 15 min to denature the DNA, and washed with sodium borate (pH 8.5). The neutralized cells were immunostained with anti-BrdU (Roche) antibody. For triple-staining with anti-DDX1, anti-hnRNP K and anti-CstF-64 (see Figure 3E), cells were fixed in 1% paraformaldehyde and incubated with rabbit anti-hnRNP K, and mouse anti-CstF-64 antibodies, followed by secondary antibody staining. Cells were then washed with PBS, fixed in 1% paraformaldehyde, and incubated with rabbit anti-DDX1 antibody directly conjugated to Alexa Fluor 647 dye (Molecular Probes).

Fluorescence Microscopy

Cells were viewed on a Zeiss LSM 510 confocal laser scanning microscope (Thornwood, NY) with a plan apochromat 63× (NA 1.4) oil immersion lens. Images from individual channels were collected sequentially in order to avoid signal bleed-through. All parameters (gain/offset value, laser intensity, and pinhole settings) were maintained constant during image acquisitions. Frame size and zoom factor were set to meet Nyquist sampling criteria. Image stacks (z-series) were taken at 0.3-μm intervals.

To determine the 3D spatial relationships between the different types of nuclear bodies, cell images were three-dimensionally reconstructed in Imaris (version 4.1.1, Bitplane AG, Zurich, Switzerland). For each image set, a background value was determined using Metamorph (Universal Imaging, Downingtown, PA). To do this, a region was drawn in an area where there were no cells, and an average value of pixel intensity for each channel was calculated. The image was then background-corrected by subtracting the background values from the image. To remove noise from the detector, a 3 × 3 × 1 median filter was applied to each image. Each image was then surface rendered (surpass mode in Imaris) using intensity threshold values specific to each antibody. These values were determined by comparing number of nuclear bodies defined at specific threshold values with the number of clearcut foci observed under the microscope. These threshold values were used as guides throughout the analysis. A minimum of 30 cells were three-dimensionally reconstructed and examined for each triple-labeling experiment at each time point.

The method of Grande *et al.* (1996) was used to estimate the probability of random association between nuclear bodies. The probability of random association between two nuclear bodies was determined using the formula $p = (4/3) \times \pi \times (d)^3 \times n \times m/v$, where d is the distance between the centers of two adjacent nuclear bodies, n and m are the average number of each nuclear body per nucleus, and v is the volume of nucleus in cubic micrometers. The probability of random association between three nuclear bodies was deter-

mined by first determining p_1 and p_2, each of which represent the probability of two nuclear bodies randomly associating (with p_1 and p_2 measuring the two different sets of nuclear body pairs). p_1 was multiplied by p_2 to get the probability of three nuclear body randomly associating with each other.

Immunoelectron Microscopy

HeLa cells were fixed in a mixture of 4% paraformaldehyde and 0.1% glutaraldehyde in Tris-phosphate buffer, pH 7.5, for 1 h. Cells were dehydrated in graded ethanol and embedded in Unicryl resin. For immunocytochemical labeling, sections on nickel grids were placed on drops of 1% bovine serum albumin in Tris-phosphate buffer for 10 min to block nonspecific binding sites. The grids were placed on drops of anti-DDX1 antibody (1/100 dilution) for 1 h, washed, and floated on drops containing Fab(2)-gold particles (10 nm; Electron Microscopy Sciences, Hatfield, PA). Labeled grids were examined using a Hitachi H7000 electron microscope (Rexdale, Ontario, Canada). The specificity of immunostaining was verified by omitting the anti-DDX1 antibody.

Western Blot Analysis

For analysis of DDX1 and CstF-64 protein during different stages of the cell cycle, whole-cell extracts were prepared by resuspending the cells in 10 mM HEPES-NaOH, pH 7.9, 1.5 mM MgCl$_2$, 10 mM KCl, 0.5 mM DTT, 0.5 mM phenylmethylsulfonyl fluoride and lysing cells in an equal volume of 50 mM Tris-HCl, pH 8.0, 1% SDS followed by syringing through a 23-gauge needle. Whole-cell extracts were electrophoresed on a SDS-10% polyacrylamide gel followed by transfer onto nitrocellulose. Blots were immunostained with rabbit anti-DDX1 antibody (2910), mouse anti-CstF-64 antibody or goat anti-actin antibody (Santa Cruz Biotechnology).

RESULTS

Association of DDX1 Bodies with Cleavage Bodies, Cajal Bodies, and Gems during the Cell Cycle

To determine the number of DDX1 bodies, cleavage bodies, CBs, and gems at different stages of the cell cycle, HeLa ATCC cells were examined in early G1 (11 h), early S (1 h), mid-S (3 h), late S (5 h), early G2 (6 h), and mid-G2 (8 h). Synchronized cells were triple-labeled with antibodies to the following: 1) DDX1 (DDX1 bodies), CstF-64 (cleavage bodies), and CPSF-100 (cleavage bodies); 2) DDX1, CPSF-100, and Sm (CBs); 3) DDX1, CstF-64, and either Sm or SMN (gems); and 4) DDX1, Sm, and SMN and examined by confocal laser scanning microscopy. In early G1, 87% of cells had DDX1 bodies with an average of 1.7 per cell, 92% of cells had CBs with an average of 3.8 per cell, and 93% of cells had gems with an average of 4.0 per cell (Table 1). Slight increases in the average numbers of DDX1 bodies, CBs, and gems were observed at early S (Table 1). These numbers did not change appreciably from mid-S to mid-G2 phases of the cell cycle. In contrast, there was an average of 1.2 CPSF-100-containing cleavage bodies at G1, with ~60% of cells having at least one CPSF-100-containing cleavage body. By early S, >90% of cells had CPSF-100-containing cleavage bodies, with an average of 2.8 per cell. These numbers remained constant until mid-G2. The most dramatic cell cycle-dependent change in nuclear body number was observed with CstF-64, with 5 and 24% of cells having at least one CstF-64-containing cleavage body (with averages of 0.1 and 0.4 per cell) in early G1 and early S, respectively. The number of CstF-64-containing cleavage bodies per cell peaked at mid-S with an average of 2.4 (95% positive cells), followed by a decrease to 1.4 (67% positive cells) by late S. By early G2, 14% of cells had at least one CstF-64-containing cleavage body with an average of 0.3 per cell, with a further reduction to 0.1 (3% positive cells) by mid-G2.

To investigate the spatial relationships between the different types of nuclear bodies, we used Imaris software to three-dimensionally reconstruct the images of nuclear bodies, as described in *Materials and Methods*. Using this program, we define two types of associations between nuclear bodies: 1) colocalization with extensive or complete overlap

Table 1. Associations between DDX1 bodies, cleavage bodies, Cajal bodies, and gems in HeLa ATCC cells during the cell cycle

Cell cycle phase[b]	DDX1 bodies (DDX1)[a]	Cleavage bodies [a]		CBs (Sm)[a]	Gems (SMN)[a]	% DDX1 bodies associated with cleavage bodies containing CPSF-100[c]	% CBs associated with gems[d]	% DDX1 bodies associated with cleavage bodies containing CPSF-100 and CBs/gems[e]
		CPSF-100	CstF-64					
Early G1 (11 h)	1.7 (0–6)	1.2 (0–5)	0.1 (0–2)	3.8 (0–7)	4.0 (0–8)	16 (2)	89	9 (2)
Early S (1 h)	2.4 (0–4)	2.8 (0–7)	0.4 (0–4)	4.7 (1–9)	5.2 (1–7)	83 (17)	84	72 (17)
Mid-S (3 h)	2.5 (0–5)	2.9 (0–7)	2.4 (0–5)	4.9 (0–7)	4.9 (1–7)	94 (80)	95	68 (72)
Late S (5 h)	2.8 (0–5)	2.6 (0–6)	1.4 (0–4)	4.1 (1–9)	3.9 (2–7)	84 (42)	90	65 (33)
Early G2 (6 h)	2.8 (0–5)	2.5 (1–5)	0.3 (0–5)	4.1 (0–7)	4.5 (0–9)	82 (6)	90	58 (3)
Mid-G2 (8 h)	2.7 (0–6)	2.6 (0–5)	0.1 (0–5)	4.3 (0–7)	4.3 (0–9)	86 (3)	89	55 (1)

A minimum of 30 cells were three-dimensionally reconstructed and examined for each triple-labeling experiment at each time point.

[a] Average number of nuclear bodies per cell with the range of nuclear bodies in cells analyzed in parentheses.

[b] Time after release in parentheses.

[c] Percentage of DDX1 bodies that associate with cleavage bodies (shown by CPSF-100 staining, with CstF-64 staining values in parentheses), with colocalization being the predominant pattern (97% of associations).

[d] Percentage of CBs that associate with gems, with colocalization being the predominant pattern (95% of associations).

[e] Percentage of DDX1 bodies that associate with cleavage bodies (shown by CPSF-100 staining or CstF-64 staining, with CstF-64 staining values in parentheses) and CBs/gems (with ~90% of colocalizing DDX1 bodies/cleavage bodies being adjacent to CBs/gems).

and 2) adjacent localization with minimal overlap. As predicted based on previous reports (Matera and Frey, 1998; Carvalho et al., 1999; Young et al., 2000), ~90% of CBs colocalized with gems in G1, S, and G2 phases of the cell cycle (Table 1). The percentage of colocalizing DDX1 bodies and CPSF-100-containing cleavage bodies was equally high, except in early G1 when only 16% colocalization was observed. In contrast, associations between DDX1 bodies and CstF-64-containing cleavage bodies were rarely observed in early G1 (2%), early G2 (6%), and mid-G2 (3%) phases of the cell cycle. In mid-S, 80% of DDX1 bodies colocalized with CstF-64-containing cleavage bodies, whereas in late S, there was 42% colocalization.

Because CBs colocalize with gems and DDX1 bodies generally colocalize with CPSF-100/CstF-64-containing cleavage bodies during S and CPSF-100-containing cleavage bodies during G2, we next studied associations between DDX1 bodies, cleavage bodies, and CBs/gems. In G1, only 9% of DDX1 bodies associated with CPSF-100-containing cleavage bodies and CBs/gems. The remaining 91% of DDX1 bodies failed to associate with either CPSF-100-containing cleavage bodies or CBs (Table 1; Figure 2, A and B). In keeping with the low percentage of CstF-64-containing cleavage bodies during early G1, 98% of DDX1 bodies showed no association with CstF-64-containing cleavage bodies and gems (Table 1; Figure 2C).

In early S phase, triple associations between DDX1 bodies, CPSF-100-containing cleavage bodies, and CBs/gems were common, with 72% of DDX1 bodies colocalized with CPSF-100-containing cleavage bodies, which in turn were found adjacent to CBs/gems (Table 1). Triple associations were considerably less frequent (17% of DDX1 bodies) when cleavage bodies were detected with anti-CstF-64 antibody. By mid-S, 80–90% of DDX1 bodies colocalized with both CstF-64- and CPSF-100-containing cleavage bodies, and DDX1 bodies/cleavage bodies were commonly found adjacent to CBs and gems (Figure 3, A and B). A three-dimensional reconstruction of the typical DDX1 body/cleavage body/CB association observed during mid-S is shown in Figure 4A. Within the limits of resolution of light microscopy, DDX1 and CstF-64 are shown as occupying the same space, whereas Sm has an adjacent location. Similar associ-

ations were observed at late S, early G2, and mid-G2 (Figure 3C), except that CstF-64-containing cleavage bodies were rarely seen in G2 (Figure 3D).

The method of Grande et al. (1996), described in *Materials and Methods*, was used to estimate the probability that three nuclear bodies would randomly associate. At mid-S, the average numbers of DDX1 bodies, CPSF-100-containing cleavage bodies, and CBs are 2.5, 2.9, and 4.9, respectively (Table 1). The volume of the nucleus in S phase HeLa cells is ~900 μm^3 (Yang et al., 1997). Using an estimated 0.5 μm as the distance between the centers of two nuclear bodies, the probability of random associations between DDX1 bodies, cleavage bodies, and CBs is <1 event in 1000 nuclei. Similar results were obtained for DDX1 bodies, cleavage bodies and gems. As ~80% of cells (70% of DDX1 bodies) show triple associations in mid-S, we propose that association between the different nuclear bodies may be of either functional or structural significance.

Association of Nuclear Bodies in HeLa PV Cells

HeLa PV differs from Hela ATCC in that gems (SMN foci) frequently reside adjacent to (rather than colocalize with) CBs in these cells (Liu and Dreyfuss, 1996). We therefore examined associations between DDX1 bodies, CstF-64- or CPSF-100-containing cleavage bodies, gems, and CBs in this cell line. As shown in Table 2, associations between nuclear bodies were less frequent in HeLa PV cells than in HeLa ATCC cells. Important differences noted in HeLa PV compared with HeLa ATCC include the following: 1) with a single exception out of >120 cells analyzed, CstF-64-containing cleavage bodies were not detected at any phase of the cell cycle; 2) CPSF-100-containing cleavage bodies were not detected in G1, but were found in low numbers (average of 0.2 per cell) in S and G2; 3) DDX1 bodies were found in reduced numbers throughout the cell cycle, with averages of 0.2, 0.6, and 0.5 per cell at G1, S, and G2, respectively; 4) numbers of CBs and gems were also reduced throughout the cell cycle; 5) the percentage of CBs that associated with gems was 35–67%, depending on the stage of the cell cycle, with adjacent localization being the predominant pattern (~70% of associations); 6) the percentage of DDX1 bodies that associated with CPSF-100-containing cleavage bodies was
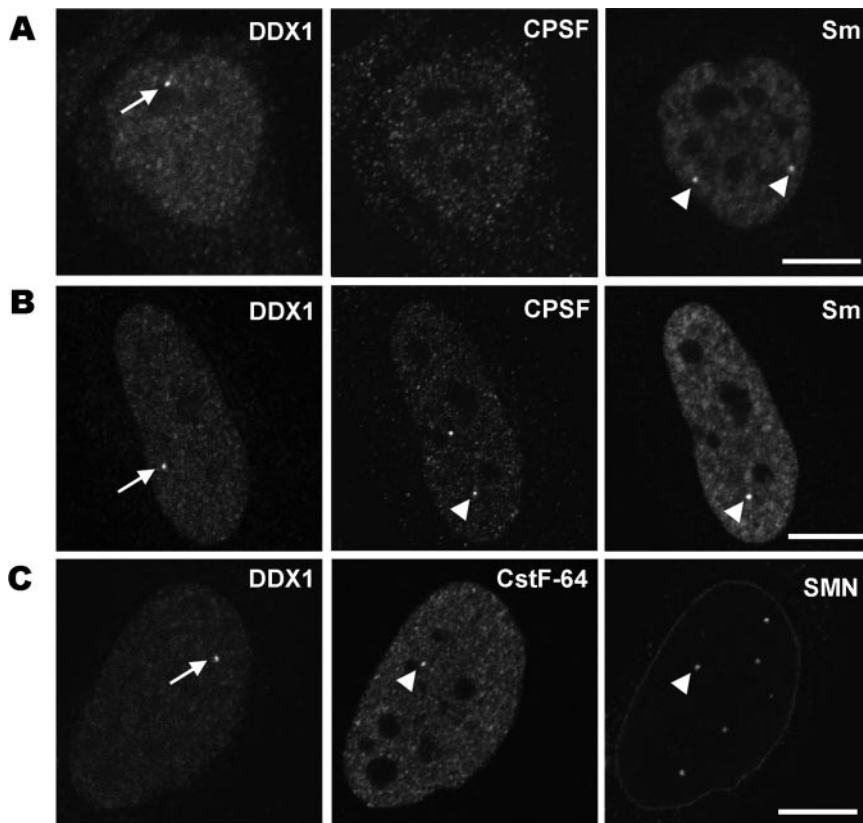
Figure 2. Association of DDX1 bodies, CBs, and gems in early G1 phase. HeLa ATCC cells were synchronized using the double thymidine block method. Eleven hours after release, cells were fixed with 1% paraformaldehyde and triple-stained with (A) anti-DDX1, anti-CPSF-100, and anti-Sm antibodies, (B) anti-DDX1, anti-CPSF-100, and anti-Sm antibodies, and (C) anti-DDX1, anti-CstF-64, and anti-SMN antibodies. Arrows, DDX1 bodies; arrowheads, cleavage bodies, CBs, or gems that are not associated with DDX1 bodies. Scale bar, 10 μm.

~20% during S and G2, with colocalization observed in ~60% of cases; and 7) the number of triple associations between DDX1 bodies, gems, and CBs was 31% in S phase (8 triple associations out of a total of 26 DDX1 bodies observed in 45 cells) and 61% (11 triple associations out of a total of 18 DDX1 bodies observed in 34 cells) in G2 phase. A three-dimensional reconstruction of a typical DDX1, SMN, and Sm triple association in HeLa PV is shown in Figure 4B, with all three nuclear bodies having an adjacent location relative to each other.

Association of Nuclear Bodies in GM38, COS7, MDCK, and NIH3T3 Cells

To further investigate nuclear body associations in human cells, we extended our analysis to the normal human fibroblast strain GM38. GM38 was triple-stained with anti-DDX1, anti-CstF-64, and anti-SMN antibodies and examined by indirect immunofluorescence. All four types of nuclear bodies were relatively rare in cycling GM38 fibroblasts. However, close associations between DDX1 bodies, CstF-64-containing cleavage bodies, and gems were still commonly observed in GM38 fibroblasts with DDX1 bodies/cleavage bodies residing adjacent to gems (Figure 5A). To enrich for cells in S phase, GM38 fibroblasts were exposed to two 16-h rounds of thymidine. BrdU incorporation was used as a marker for cells in S phase. Three hours after the second thymidine block, 62% of GM38 fibroblasts were in S phase compared with 21% in an unsynchronized cell population, as revealed by BrdU staining. Consistent with these numbers, 67% of S-phase-synchronized GM38 fibroblasts had CstF-64-containing cleavage bodies, most of which colocalized with DDX1 foci. The majority of DDX1 bodies/cleavage bodies were found adjacent to gems.

Next, we studied the SV40-transformed monkey kidney cell line COS7. More than 60% of cells analyzed contained DDX1 and CstF-64-containing cleavage bodies with the predominant form of association being colocalization. Although CBs and gems were less commonly observed in COS7 cells, they frequently colocalized with each other (Figure 5B). However, in contrast to HeLa and GM38 cells, only ~10% DDX1 bodies associated with CBs/gems (Figure 5B). We also examined MDCK (Madin-Darby canine kidney) cells and NIH3T3 mouse fibroblasts for nuclear body associations. DDX1 bodies were only found in ~30–40% of cells. Although CstF-64 aggregates were observed in MDCK and NIH3T3 cells, there were no distinctive CstF-64-containing cleavage bodies in these two cell lines. Associations between DDX1 bodies and gems were occasionally observed in MDCK cells and were absent in NIH3T3 cells (unpublished data).

Structural Characterization of DDX1 Bodies

In a previous study, we postulated that DDX1 might be a constituent of cleavage bodies (Bleoo *et al.*, 2001). However, the work described here suggests that DDX1 bodies often exist independent of CstF-64- and CPSF-100-containing cleavage bodies, especially during G1 phase (Figure 2). To further characterize DDX1 bodies, we examined whether hnRNP K, a protein previously shown to coimmunoprecipitate with DDX1 (Chen *et al.*, 2002), is also found in DDX1 bodies. Because both anti-DDX1 and anti-hnRNP K antibodies were prepared in rabbit, we first costained HeLa ATCC cells in mid-S phase with either anti-hnRNP K and anti-CstF-64 antibodies, or anti-DDX1 and anti-CstF-64 antibodies. Colocalization of hnRNP K and CstF-64 within the same nuclear bodies was observed at the same frequency as that of
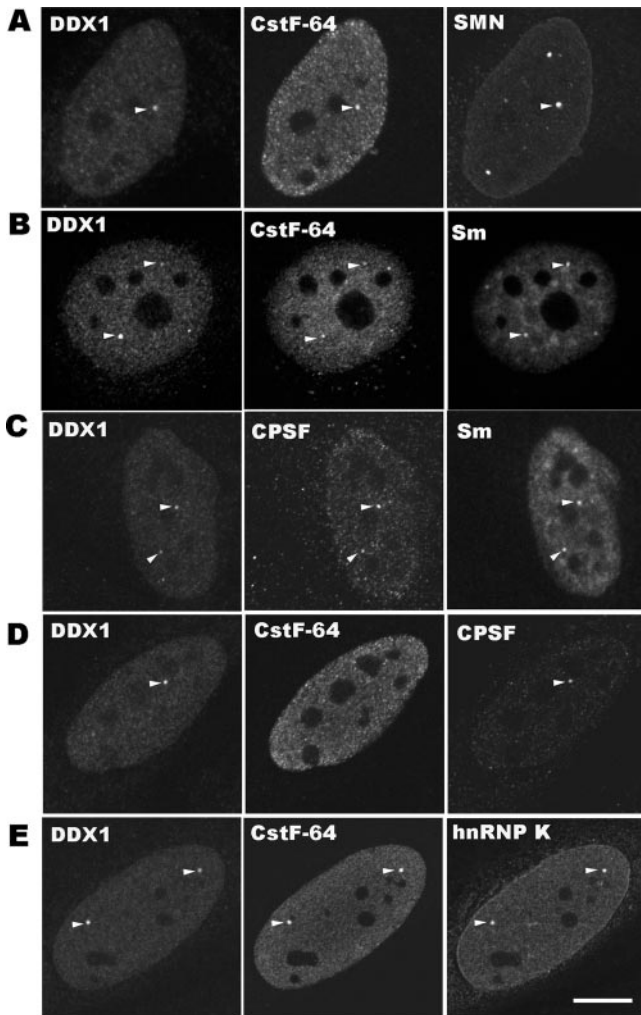
Figure 3. Triple associations of DDX1 bodies, cleavage bodies, and either CBs or gems at mid-S and early G2 phases. (A and B) For mid-S phase, HeLa ATCC cells were fixed 3 h after release from the double thymidine block and triple-stained with anti-DDX1, anti-CstF-64, and anti-SMN antibodies (A) or anti-DDX1, anti-CstF-64, and anti-Sm antibodies (B). Arrowheads indicate DDX1 bodies that colocalize with cleavage bodies, which in turn are adjacent to gems in A and CBs in B as determined by confocal microscopy. (C and D) For early G2 phase, HeLa ATCC cells were fixed 6 h after release from the second thymidine block and triple-stained with anti-DDX1, anti-CPSF-100, and anti-Sm antibodies (C) or anti-DDX1, anti-CstF-64, and anti-CPSF-100 antibodies (D). During early G2, CPSF-100-containing cleavage bodies remained associated with DDX1 bodies and CBs (C), whereas CstF-64-containing cleavage bodies disappeared (D; arrowheads in C and D). (E) HeLa cells in mid-S phase were triple-stained with anti-DDX1, anti-CstF-64, and anti-hnRNP K antibodies. Arrowheads in E indicate colocalization. Scale bar, 10 μm.

DDX1 and CstF-64. Next, we directly conjugated anti-DDX1 antibody with Alexa 647 and immunostained HeLa ATCC cells in mid-S phase with directly conjugated anti-DDX1, anti-CstF-64, and anti-hnRNP K antibodies. All three proteins were found within the same nuclear bodies in ~90% of cells.

Electron microscopy was used to examine the ultrastructure of DDX1 bodies. Thin sections of HeLa ATCC cells on nickel grids were first incubated with anti-DDX1 antibody, followed by 10-nm Fab(2)-gold particles. Based on number
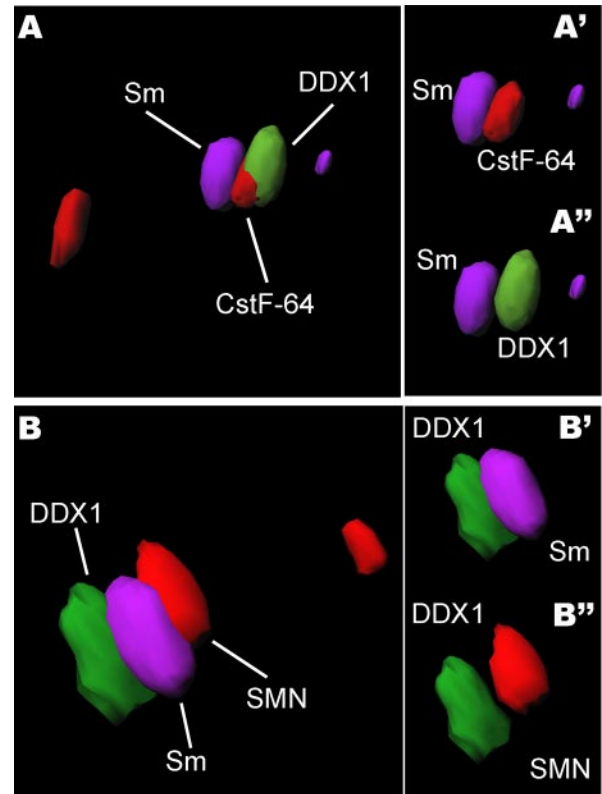
Figure 4. (A) Association between DDX1 bodies (green), cleavage bodies (red), and Cajal bodies (purple) during S-phase in HeLa ATCC cells. The images of different types of nuclear bodies were three-dimensionally reconstructed using surface rendering techniques with the Imaris program (version 4.1.1, Bitplane AG). (A) Cleavage bodies predominantly colocalized with DDX1 bodies, whereas CBs (and gems) were mostly found adjacent to DDX1. To better illustrate the spatial relationship between DDX1 bodies and cleavage bodies, only two types of nuclear bodies are shown in A' (CB and cleavage body) and A" (CB and DDX1 body). Removal of the green channel (DDX1) reveals the entire shape of the cleavage body, whereas removal of the red channel (CstF-64) reveals the entire shape of the DDX1 body. (B) Association between DDX1 bodies (green), CBs (purple), and gems (red) during S phase of the cell cycle in HeLa PV cells. All three nuclear bodies have an adjacent association, as illustrated in B' and B".

of gold particles, DDX1 proteins are relatively abundant and evenly distributed within DDX1 bodies (Figure 6). Furthermore, DDX1 bodies are roughly circular with a diameter of ~0.5 μm. As with other nuclear bodies, DDX1 bodies are located within densely staining regions of the nucleus.

Analysis of CstF-64 and DDX1 Protein Levels during the Cell Cycle
CstF-64-containing cleavage bodies are rarely seen outside S phase in HeLa ATCC and GM38 cells. The S phase-specific increase in the number of CstF-64-containing cleavage bodies could result from either an increase in overall levels of CstF-64 or their redistribution. In support of the former, Martincic et al. (1998) have previously reported a fivefold increase in CstF-64 protein levels during the G0 (serum-starved) to S phase transition in mouse 3T6 fibroblasts. To examine whether CstF-64 protein levels change during the cell cycle, we prepared whole-cell extracts from synchronized HeLa ATCC cells immediately after release from the

Table 2. Associations between DDX1 bodies, cleavage bodies, Cajal bodies, and gems in HeLa PV cells during the cell cycle

Cell cycle phase[a]	DDX1 bodies (DDX1)[b]	Cleavage bodies (CPSF-100)[b]	CBs (Sm)[b]	Gems (SMN)[b]	% DDX1 bodies associated with cleavage bodies[c,d]	% DDX1 bodies[d,e]		% CBs associated with gems[d,f]	% DDX1 bodies associated with CBs and gems[d,g]
						Associated with CBs	Associated with gems		
Early G1 (11 h)	0.2 (0–2)	ND	1.5 (0–3)	2.6 (0–7)	ND (0/14)	ND (0/8)	ND (0/8)	35 (19/54)	ND (0/14)
Mid-S (3 h)	0.6 (0–2)	0.2 (0–2)	1.5 (0–3)	2.0 (0–4)	24% (5/21)	42% (11/26)	38% (10/26)	41 (21/51)	31 (8/26)
Early G2 (6 h)	0.5 (0–2)	0.2 (0–1)	1.7 (0–4)	2.7 (0–5)	21% (3/14)	67% (12/18)	61% (11/18)	67 (39/58)	61 (11/18)

A minimum of 35 cells were three-dimensionally reconstructed and examined for each triple-labeling experiment at each time point. ND, not detected.

[a] Time after release in parentheses.

[b] Average number of nuclear bodies per cell with the range of nuclear bodies in cells analyzed in parentheses.

[c] Percentage of DDX1 bodies that are associated with cleavage bodies (shown by CPSF-100 staining), with colocalization being the predominant pattern (~60% of associations).

[d] Parentheses indicate number of associations per total number of nuclear bodies examined.

[e] Percentage of DDX1 bodies that are associated with CBs or gems, with adjacent localization being the predominant pattern (~70% of associations).

[f] Percentage of CBs that are associated with gems, with adjacent localization being the predominant pattern (~70% of associations).

[g] Percentage of DDX1 bodies that are associated with CBs and gems, with adjacent localization being the predominant pattern (~70% of associations).

second thymidine block (0 h) and at 1, 3, 4, 5, 6, 8, 10, and 11 h after thymidine block release. As shown in Figure 7, there was no significant change in overall CstF-64 levels during the cell cycle. As expected based on our previous report, there was no change in DDX1 levels during the cell cycle (Bleoo *et al.,* 2001).

Absence of RNA in DDX1 Bodies and Cleavage Bodies
Previous studies have shown that there is no newly synthesized RNA in CBs (Raska, 1995; Schul *et al.,* 1996), although snRNPs are associated with CBs (Wu *et al.,* 1991; Carmo-Fonseca *et al.,* 1992). In contrast, Schul *et al.* (1996) have reported that ~20% of cleavage bodies contain nascent RNA in unsynchronized T24 cells. To address whether nascent RNAs are present in cleavage bodies during the S phase of the cell cycle, we labeled HeLa ATCC cells with 5-FU for 15 min during mid-S phase (3 h after release of the second thymidine block). Of 50 cells analyzed, none showed significant 5-FU labeling in cleavage bodies (Figure 8A). To de-

termine whether mature RNAs are found in cleavage bodies, HeLa ATCC cells in mid-S phase were pulsed with 5-FU for 10 min and incubated for an additional 40 min before immunostaining. Although the overall RNA signal was stronger in these cells than in the previous experiment, there was no accumulation of 5-FU in cleavage bodies (Figure 8B). Our results suggest that cleavage bodies are devoid of RNAs during S phase, consistent with our previous report indicating that RNA is not found within DDX1 bodies and cleavage bodies in unsynchronized cells (Bleoo *et al.,* 2001).

Effect of Inhibiting RNA Transcription and DNA Replication on Nuclear Bodies
Inhibition of transcription using actinomycin D disrupts CBs and gems (Carmo-Fonseca *et al.,* 1992; Liu and Dreyfuss, 1996). To pursue the possibility that active transcription is required for the specific types of associations observed between nuclear bodies during S phase, we treated S phase
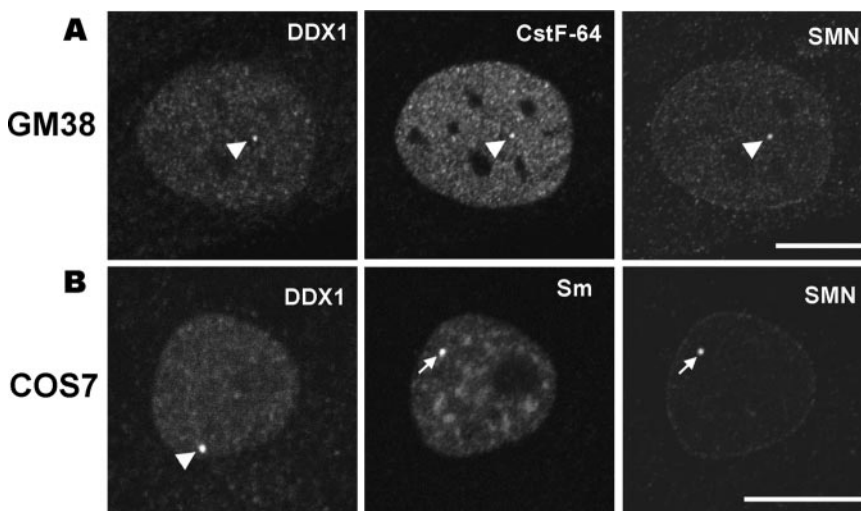
Figure 5. Colocalization of nuclear bodies in normal human GM38 fibroblasts and COS7 cells. (A) GM38 fibroblasts were fixed with 1% paraformaldehyde and triple-stained with anti-DDX1, anti-CstF-64, and anti-SMN antibodies. Nuclear body associations are indicated by the arrowheads. (B) COS7 cells were fixed with 1% paraformaldehyde and triple-stained with anti-DDX1, anti-Sm, and anti-SMN antibodies. The arrowhead points to the DDX1 body, whereas the arrows indicate colocalization of the CB and gem. Scale bar, 10 μm.
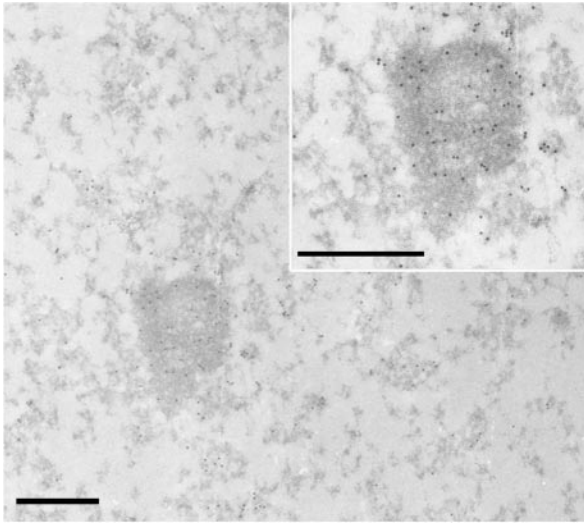
Figure 6. Ultrastructural analysis of a DDX1 body. Thin sections of HeLa ATCC cells were incubated with anti-DDX1 antibody and 10-nm F(ab)2-gold particles. Cells were scanned for the presence of DDX1 aggregates using a Hitachi H7000 electron microscope. A magnification of the DDX1 body is shown in the inset. Scale bar, 0.5 μm.

HeLa ATCC cells with 6 μg/ml actinomycin D, a concentration that inhibits RNA polymerase I, II, and III. Consistent with previous reports, actinomycin D treatment caused disruption of CBs and gems (unpublished data). However, DDX1 bodies and CstF-64-containing cleavage bodies were not altered as the result of transcription inhibition and remained associated (unpublished data). Similar results were observed with 50 μg/ml α-amanitin, which specifically inhibits RNA polymerase II (unpublished data).

The convergence of DDX1 bodies, cleavage bodies, CBs, and gems by early S phase is intriguing, especially in light of the fact that the great majority of nuclear body associations have the same configuration; i.e., DDX1 bodies colocalize with cleavage bodies, with gems and CBs having an adjacent location to the other two nuclear bodies. Furthermore, the
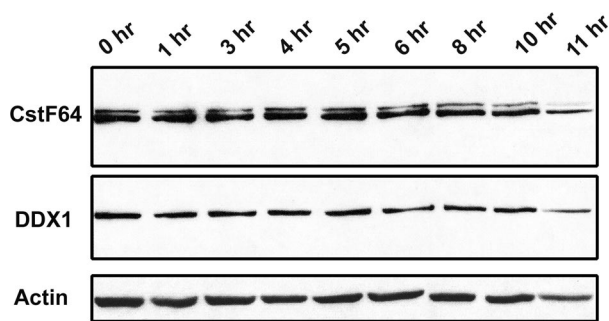
Figure 7. Western blot analysis of CstF-64 and DDX1 protein levels during the cell cycle. Synchronized HeLa ATCC cells were harvested at the indicated time points after release from the second thymidine block. Whole-cell extracts (40 μg/lane) were electrophoresed through a 10% SDS-PAGE gel and electroblotted onto nitrocellulose. CstF-64 was detected using a 1:1000 dilution of mouse monoclonal anti-CstF-64 antibody, whereas DDX1 was detected using a 1:5000 dilution of rabbit polyclonal anti-DDX1 antibody. Actin was visualized using a 1:500 dilution of goat polyclonal anti-actin antibody.

pattern of CstF-64 appearance and disappearance in cleavage bodies as the cell cycle progresses from mid-S to late S to early G2 suggests a specific need for CstF-64 during S phase. As DNA replication is the hallmark of S phase, we addressed the possibility that DNA replication might be involved in either association of cleavage bodies with DDX1 bodies, CBs, and gems, or the aggregation of CstF-64 protein within cleavage bodies. HeLa ATCC cells in S phase were treated with aphidicolin, an inhibitor of eukaryotic DNA polymerase α, δ, and ϵ (Burgers and Bauer, 1988). As shown in Figure 9, aphidicolin efficiently inhibited DNA replication, as revealed by the lack of BrdU incorporation. Although DDX1 bodies, CBs, and gems were not affected by inhibition of DNA replication, a dramatic decrease in the number of CstF-64-containing cleavage bodies was observed (Figure 9). Only 24% (25/105) of cells retained CstF-64-containing cleavage bodies after aphidicolin treatment, compared with 98% (98/100) in untreated control cells. Furthermore, a reduction in the size of CstF-64-containing cleavage bodies was observed in the 24% of cells that retained these nuclear structures. An interesting finding is that when we replaced anti-CstF-64 antibody with anti-CPSF-100 antibody in these experiments, CPSF-100-containing cleavage bodies appeared completely normal, suggesting that the effect observed on inhibition of DNA replication is related to CstF-64 and not to cleavage bodies per se (Figure 9B). Next, we treated S-phase cells with hydroxyurea (HU), a drug that blocks DNA replication by inhibiting the activity of ribonucleotide reductase (Thelander and Reichard, 1979). After HU treatment, only 38% cells retained CstF-64-containing cleavage bodies, supporting a special link between CstF-64 aggregation into cleavage bodies and DNA replication.

To determine whether the CstF-64-specific effect observed upon inhibition of DNA replication might be mediated through close proximity or association with nascent DNA, HeLa ATCC cells were labeled with BrdU for 30 min during mid-S phase (3 h after release of the second thymidine block). Of >20 cells analyzed, none showed significant BrdU incorporation in cleavage bodies (Figure 8C).

Effects of Inhibiting Actin Polymerization on Nuclear Bodies

The nonrandom nuclear body associations observed during S phase suggest directed and regulated movement within the nucleus. In the cytoplasm, actin and microtubule motors are responsible for moving organelles along filaments (reviewed in Ehrenberg and McGrath, 2004). Actin also plays important roles in the nucleus (e.g., in chromatin remodeling, transcription, and RNA transport), although it is still not known whether actin exists in a filamentous state in the nucleus (reviewed in Bettinger *et al.*, 2004). Of note, filaments believed to be composed of actin were found to be embedded into CBs by immunogold labeling (Kiseleva *et al.*, 2004). Furthermore, Gedge *et al.* (2005) have reported that nuclear actin partially colocalizes with CBs in cultured human cells. We therefore used two inhibitors of actin polymerization, latrunculin B, which inhibits actin polymerization by sequestering actin monomer (Coue *et al.*, 1987; Spector *et al.*, 1989), and cytochalasin D, which binds to the barbed end of actin filaments (Cooper, 1987), to examine whether either the formation of nuclear bodies or the association between nuclear bodies during S phase was dependent on an actin polymer.

After latrunculin B treatment, DDX1 bodies, CBs, and gems remained intact (Figure 10, A and B). However, rather
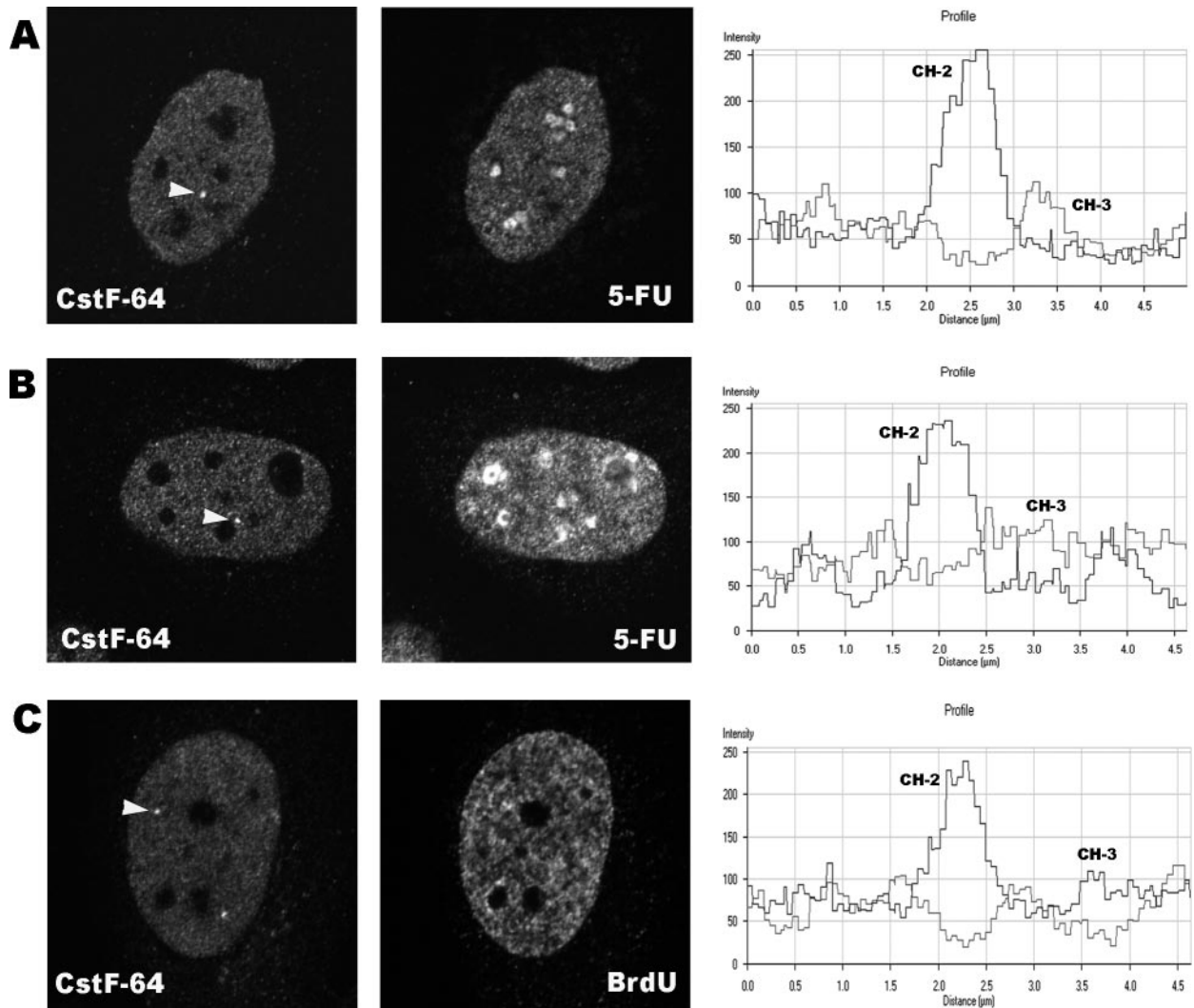
Figure 8. Absence of RNA and DNA in cleavage bodies. (A) S phase synchronized HeLa ATCC cells were incubated with 5-FU for 15 min and immunostained with anti-CstF-64 and anti-BrdU antibodies. Staining intensity through a cleavage body (arrowhead) and surrounding region was profiled with Zeiss LSM 510 image software. Channel 2 (CH-2) and channel 3 (CH-3) represent staining intensities of CstF-64 and 5-FU, respectively. (B) S phase synchronized HeLa ATCC cells were pulse-labeled with 5-FU for 10 min and incubated at 37°C for 40 min before staining with anti-CstF-64 and anti-BrdU antibodies. Staining intensity was analyzed as indicated in A. (C) S phase-synchronized HeLa ATCC cells were incubated with 200 μM BrdU for 30 min and immunostained with anti-CstF-64 and anti-BrdU antibodies. Staining intensity was analyzed as indicated in A.

than cleavage bodies, long thin needlelike structures (referred to as nuclear spicules) were observed in more than 80% of cells immunostained with either anti-CstF-64 or anti-CPSF-100 antibodies (Figure 10, A–C and E). Most cells exhibited an aberrant nuclear morphology, as expected after disruption of the cytoskeleton. Identical results were obtained using the following: 1) different concentrations of paraformaldehyde (1 and 3%), 2) different primary anti-CstF-64 antibodies, and 3) different secondary antibodies. Control experiments where cells were treated with 0.1% dimethyl sulfoxide (DMSO), the diluent used for latrunculin B, revealed normal cleavage bodies. Of note, cytochalasin D treatment (also dissolved in 0.1% DMSO) neither disrupted cleavage bodies nor resulted in the formation of nuclear spicules, even though cytoplasmic filamentous actin could no longer be visualized by phalloidin staining (Figure 10D). Decreasing the concentration of latrunculin B (to 2 μM) or increasing the con-

centration of cytochalasin D (to 40 μM) generated the same results as obtained with the original drug concentrations (unpublished data).

To determine whether nuclear spicules are S phase-specific, we analyzed unsynchronized HeLa ATCC cells. We found that the number of unsynchronized cells with nuclear spicules was much higher (~70%) than the number of cells in S phase (29%; Figure 1). A high percentage of cells with nuclear spicules was also observed in unsynchronized GM38 treated with latrunculin B (unpublished data). We then examined whether the formation of nuclear spicules was transcription-dependent. HeLa ATCC cells were incubated with 6 μg/ml actinomycin D for 60 min before the latrunculin B treatment. The number and appearance of nuclear spicules in actinomycin D/latrunculin B-treated cells was comparable to that observed in cells treated with latrunculin B alone, indicating that these structures are not dependent on active transcription (see Figure 12, left panel).
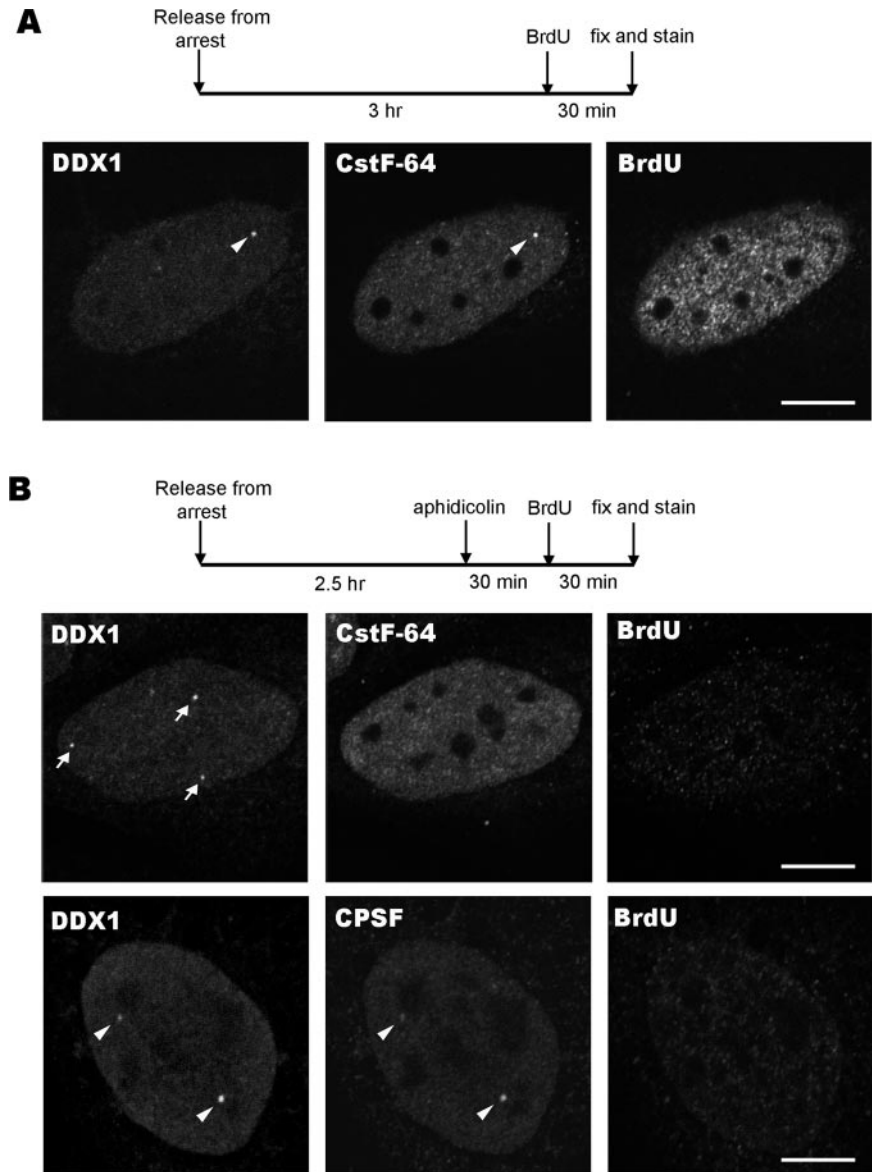
Figure 9. Inhibition of DNA replication eliminates the majority of cleavage bodies. Aphidicolin (10 μg/ml) was added to the culture medium of HeLa ATCC cells 2.5 h after release from the second thymidine block (S phase). After 30 min, BrdU was added to a final concentration of 200 μM for an additional 30 min. Cells were triple-stained with anti-DDX1, anti-CstF-64, and anti-BrdU. (A) In the absence of aphidicolin, DDX1 bodies colocalized with cleavage bodies (arrowhead). BrdU-labeled DNA was found throughout the nucleus. (B) In the presence of aphidicolin, DNA replication was inhibited as indicated by the absence of BrdU label within the nucleus. DDX1 bodies (arrowheads) and CPSF-100-containing cleavage bodies were not affected by aphidicolin treatment, although the majority of CstF-64-containing cleavage bodies disappeared. Scale bar, 10 μm.

Next, we investigated whether RNA was located along or within the nuclear spicules. We found that pulse-labeled 5-FU, but not fresh-labeled 5-FU, was present in the spicules of ~50% of cells, indicating that at least a subset of these structures contain processed but not nascent RNAs (Figure 11A). We also discovered that hyperphosphorylated RNA polymerase II, the form that is active in RNA elongation, colocalizes with CstF-64 along the spicules in ~60% of cells examined (Figure 11B). When cells were treated with actinomycin D before latrunculin B, neither hyperphosphorylated RNA polymerase II nor RNA could be detected in the nuclear spicules (Figure 12, right panel).

Because the needlelike appearance of the spicules suggests a somewhat rigid underlying filamentous structure, we examined whether either actin or nuclear intermediate filament proteins called lamins were associated with the nuclear spicules. No association was detected between nuclear actin and CstF-64-stained spicules (Figure 11C). Similarly, lamins A/C and lamin B appeared to be completely excluded from the nuclear spicules (Figure 11D and unpublished data).

DISCUSSION

Highly dynamic compartments and subdomains have been identified in the nucleus including nucleoli, splicing factor compartments believed to supply splicing factors to transcription sites, PML bodies implicated in transcriptional regulation and tumor suppression, CBs, and cleavage bodies (reviewed in Gall, 2000; Lamond and Spector, 2003; Dellaire and Bazett-Jones, 2004). Although great strides have been made in the characterization of nuclear subdomains, we still have a poor understanding of the overall structural organization of the nucleus and the roles that nuclear subdomains play in the cell.

A number of investigations have focused on three nuclear bodies that associate with each other, frequently or occasionally depending on the study: CBs, gems, and cleavage bodies. These three nuclear bodies contain proteins involved in or postulated to be involved in RNA transcription, splicing, processing, and transport. In a previous study, we identified DDX1 as a component of cleavage bodies because of its
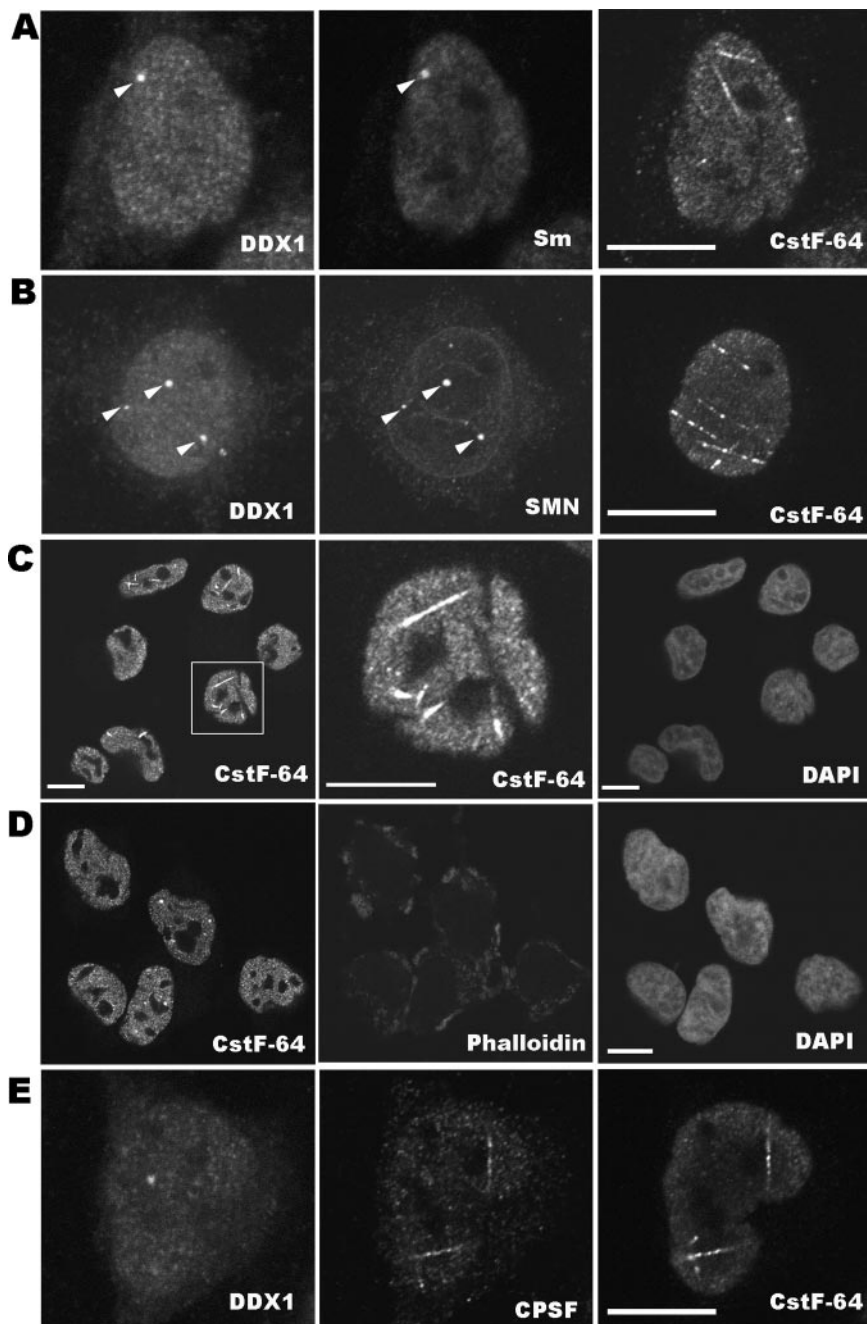
Figure 10. Inhibition of actin polymerization by latrunculin B alters cleavage bodies. S-phase synchronized HeLa ATCC cells (2.5 h after release from the second thymidine block) were treated with 5 μM latrunculin B for 40 min and immunostained with anti-DDX1, anti-Sm, and anti-CstF-64 antibodies (A) or anti-DDX1, anti-SMN, and anti-CstF-64 antibodies (B). Latrunculin B had no effect on DDX1 bodies, CBs, and gems (arrowheads indicate association between DDX1 bodies and CBs (A) and gems (B) after latrunculin B treatment), but resulted in the disappearance of cleavage bodies and the appearance of nuclear spicules. (C) HeLa ATCC cells were treated with latrunculin B and immunostained with anti-CstF-64 antibody and DAPI. A magnification of the cell highlighted in the left panel is shown in the center panel, demonstrating the typical appearance of nuclear spicules. (D) HeLa ATCC cells were treated with 20 μM cytochalasin D for 40 min and then immunostained with anti-CstF-64 antibody, phalloidin, and DAPI. There was an absence of filamentous actin in the cytoplasm of cytochalasin D-treated cells as revealed by phalloidin staining. Cytochalasin D had no effect on cleavage bodies. (E) HeLa ATCC cells were treated with latrunculin B and immunostained with anti-DDX1, anti-CPSF-100, and anti-CstF-64 antibodies. Both CstF-64 and CPSF-100 were found in nuclear spicules. Coverslips were mounted onto slides with glycerol containing 1 mg/ml ρ-phenylenediamine or with glycerol alone, with identical results. Scale bars, 10 μm.

frequent presence in these nuclear bodies (Bleoo *et al.,* 2001). The more comprehensive study described here demonstrates that DDX1 bodies can exist as entities that are separate from CPSF-100- and CstF-64-containing cleavage bodies. Furthermore, cells that do not form cleavage bodies as visualized by confocal microscopy often have well-defined DDX1 bodies. In support of an independent status for DDX1 bodies, we show that hnRNP K, previously found to coimmunoprecipitate with DDX1 (Chen *et al.,* 2002), is also present in DDX1 bodies. Ultrastructure analysis by immunogold labeling of DDX1 demonstrates that DDX1 bodies are electron-dense structures that contain a significant amount of DDX1 protein.

Here, we examine the spatial relationship between cleavage bodies, CBs, gems, and DDX1 bodies as a function of the cell cycle in HeLa ATCC cells. To avoid bias, cells were randomly selected, confocal microscopy settings were maintained throughout the analysis, and nuclear bodies were defined based on parameters established using the Imaris three-dimensional reconstruction program. Using these criteria, and in agreement with previous studies, our results indicate that: 1) DDX1 bodies, CBs, and gems are present throughout the G1, S, and G2 phases of the cell cycle (previous work has shown that DDX1 bodies, cleavage bodies and CBs disassemble during mitosis; Andrade *et al.,* 1993; Schul *et al.,* 1996; Bleoo *et al.,* 2001); 2) the number of DDX1 bodies, CBs, and gems remains constant throughout G1, S, and G2; 3) the great majority of CBs and gems colocalize with each other in G1, S, and G2; and 4) a high percentage of CBs/gems associate with DDX1 bodies during G1, S, and
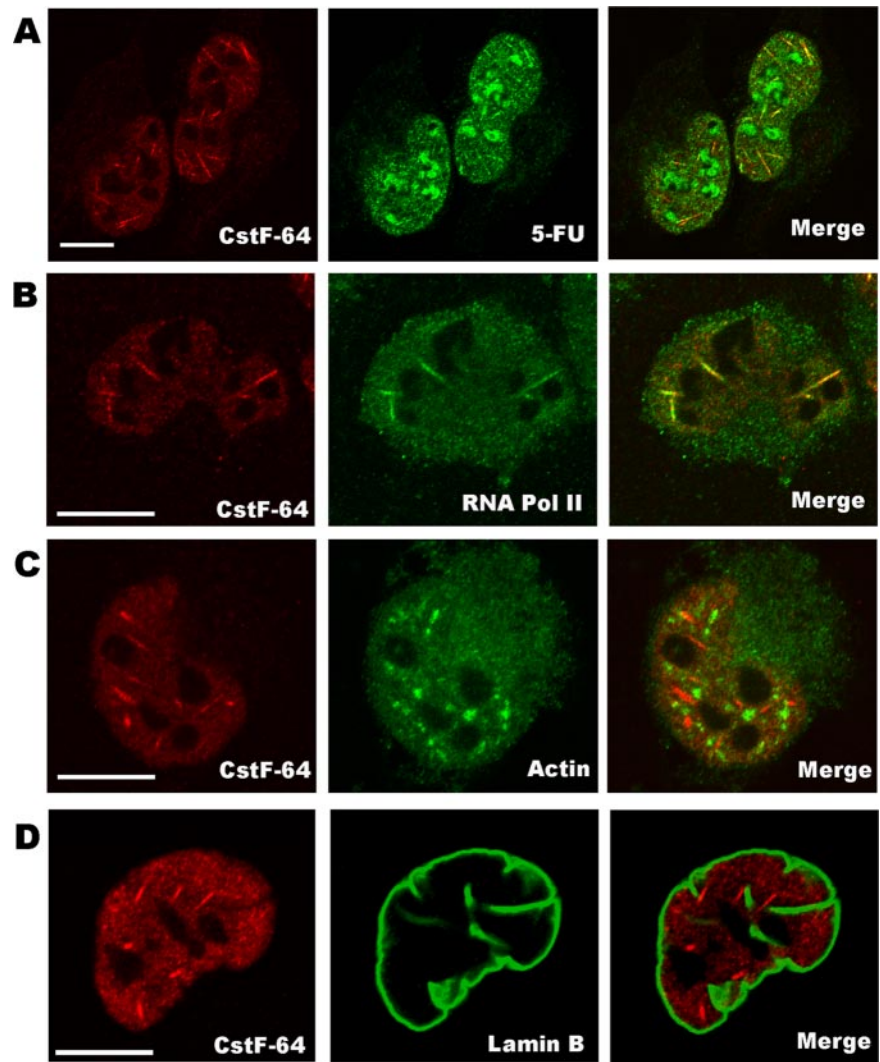
Figure 11. Association of CstF-64 and other proteins in nuclear spicules after latrunculin B treatment. (A) S-phase synchronized HeLa ATCC cells (2.5 h after release from the second thymidine block) were pulse-labeled with 1.3 μM 5-FU for 10 min and then treated with 5 μM latrunculin B for 40 min and immunostained with anti-CstF-64 (red) and anti-BrdU (green) antibodies. Colocalization of CstF-64 and RNA in the nuclear spicules generates the yellow color in the Merge panel. (B) S-phase synchronized HeLa ATCC cells were treated with 5 μM latrunculin B for 40 min and immunostained with anti-CstF-64 antibody (red) and an anti-RNA polymerase II antibody that specifically recognizes the hyperphosphorylated form of RNA polymerase II (green). The yellow color in the Merge panel indicates colocalization of CstF-64 and the hyperphosphorylated RNA polymerase II in the nuclear spicules. (C and D) Synchronized HeLa ATCC cells were treated with latrunculin B as described in B and immunostained with anti-CstF-64 (red) and either anti-actin (green; C) or anti-lamin B (green) antibodies (D). No association was found between CstF-64 and either actin or lamin B in the nuclear spicules. Scale bars, 10 μm.

G2, with an adjacent localization being the predominant pattern.

In comparison with the other three nuclear bodies, the formation and composition of cleavage bodies appears more dynamic. For example, CstF-64-containing cleavage bodies were primarily observed in mid-S and to a lesser extent in late S phase, whereas the number of CPSF-100-containing cleavage bodies doubled from early G1 to early S. The increase in the number of CstF-64-containing cleavage bodies during S phase was not accompanied by an increase in CstF-64 protein levels, suggesting redistribution of CstF-64 rather than de novo synthesis. The predominant association pattern at mid-S consisted of DDX1 bodies colocalizing with CPSF-100/CstF-64-containing cleavage bodies and residing adjacent to CBs and gems. Associations between CBs and cleavage bodies detected with either CstF-64 or CPSF-100 antibodies have previously been reported in the human bladder carcinoma cell line T24 (Schul *et al.*, 1996, 1999). In contrast to our results in HeLa ATCC and GM38, CBs were found to localize with CstF-64-containing cleavage bodies in G1 and to be adjacent during S phase in T24 cells (Schul *et al.*, 1999). This discrepancy with our results could be due to differences between cell lines as T24 has been reported to have a different nuclear body content compared with other cell lines (Grande *et al.*, 1996).

To address the nature of the associations between cleavage bodies, DDX1 bodies, gems, and CBs during S phase, synchronized cells were treated with inhibitors of RNA transcription. Although inhibitors of transcription had the expected disruptive effect on CBs and gems (Carmo-Fonseca *et al.*, 1992; Liu and Dreyfuss, 1996), neither cleavage bodies nor DDX1 bodies were affected. In contrast, inhibitors of DNA replication caused a dramatic decrease in the number of CstF-64-containing cleavage bodies although CPSF-100-containing cleavage bodies, DDX1 bodies, CBs, and gems were not affected, suggesting a specific link between CstF-64 and DNA replication. Of note, cleavage bodies in S phase appeared to be devoid of RNA and DNA as determined by labeling with 5-FU and BrdU. Together, these results indicate that although active transcription is not required for cleavage body formation and/or maintenance, inhibition of DNA replication affects their protein composition.

CstF-64 in cleavage bodies could be generally associated with DNA replication or specifically associated with the replication of a subset of DNA, although no role in DNA replication has been reported for CstF-64. Conversely, CstF-64-containing cleavage bodies may be required for processes related to DNA replication but not necessarily directly involving DNA replication. For example, in mammalian cells, CBs and cleavage bodies have both been shown to be closely
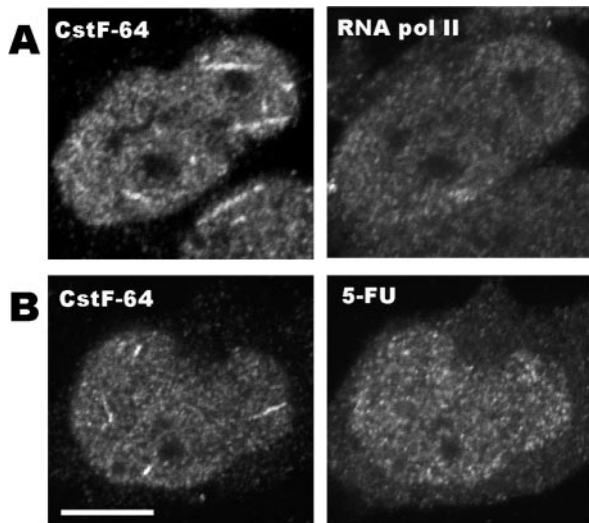
Figure 12. Nuclear spicule formation is transcription-independent but their composition is transcription-dependent. (A) HeLa ATCC cells were incubated with 6 μg/ml actinomycin D for 60 min before they were treated with 5 μM latrunculin B for 40 min. Cells were then immunostained with anti-CstF-64 and anti-RNA polymerase II antibodies. (B) HeLa ATCC cells were pulse-labeled with 5-FU for 10 min and incubated at 37°C for 40 min. Cells were then sequentially treated with actinomycin D and latrunculin B as described in A and immunostained with anti-CstF-64 antibody and anti-BrdU antibody that recognizes 5-FU. Neither RNA polymerase II nor RNA was observed in nuclear spicules. Scale bar, 10 μm.

associated with histone gene clusters that are preferentially transcribed during S phase (Frey and Matera, 1995; Schul *et al.*, 1999). Schul *et al.* (1999) have postulated that cleavage bodies function adjacent to CBs to promote histone gene transcription and/or processing. As histone gene expression and DNA replication are tightly coupled during S phase, inhibition of DNA replication affects histone gene transcription and vice versa (Heintz *et al.*, 1983; Nelson *et al.*, 2002). Thus, the disappearance of CstF-64 in cleavage bodies that we see upon inhibition of DNA replication could be related to the accompanying decrease in histone gene transcription. The fact that general inhibitors of transcription have no effect on CstF-64 distribution suggests that the requirement for CstF-64 in cleavage bodies during S phase is related to the coupling between DNA replication and histone gene transcription rather than histone gene transcription per se. Furthermore, the lack of RNA and DNA in cleavage bodies suggests that these structures do not serve as active sites of transcription or processing, but rather provide preassembled complexes or storage for molecules involved in these processes, as previously postulated for CBs and cleavage bodies (Schul *et al.*, 1998, 1999; Gall *et al.*, 1999).

Our findings suggest nonrandom associations of structural and/or functional significance between the four nuclear bodies. Nonrandom associations imply a directed, possibly motor-driven mechanism for bringing together different types of nuclear bodies, either through specific molecular interactions and/or as a consequence of movement along filamentous structures such as has been described for transporting organelles along cytoplasmic actin or tubulin fibers. Although the presence of actin in the nucleus is well documented, it is still not known whether physiologically-relevant nuclear actin filaments exist (reviewed in Pederson and Aebi, 2002; Bettinger *et al.*, 2004).

Nuclear actin has been shown to be associated with CBs (Gedge *et al.*, 2005) and pore-linked filaments believed to contain actin are embedded in CBs and other organelles (Kiseleva *et al.*, 2004). It has been postulated that rather than the well-known filamentous form of cytoplasmic actin, nuclear actin, perhaps in association with actin binding proteins that affect branching, may exist in distinct polymeric or oligomeric forms (Pederson and Aebi, 2002).

To address a possible role for polymerized actin in either the association or formation of nuclear bodies, we treated HeLa ATCC cells with latrunculin B, a compound that forms a 1:1 complex with actin monomers, thus inhibiting actin polymerization (Coue *et al.*, 1987; Spector *et al.*, 1989). Although CBs, gems, and DDX1 foci were not affected by latrunculin B, there was a dramatic change in both the CstF-64 and CPSF-100 staining patterns in more than 80% of S-phase cells examined. Rather than the spherical shape normally associated with cleavage bodies, immunostaining with anti-CstF-64 and anti-CPSF-100 revealed long thin needlelike structures (nuclear spicules) that also contained RNA polymerase II and processed RNA. We subsequently discovered that the formation of nuclear spicules is not restricted to cells in S phase. These results suggest directional aggregation of CstF-64 and CPSF-100 proteins along with RNA polymerase II upon treatment with latrunculin B. Interestingly, cytochalasin D, which binds to the barbed end of actin filaments, preventing association and dissociation of actin at that end, had no effect on cleavage bodies. As the consequence of cytochalasin D treatment in the cytoplasm is shortened actin polymers rather than total disruption of the actin polymer, the nuclear actin polymer may be less dramatically affected by cytochalasin D than by latrunculin B. Others have reported differences between cytochalasin D and latrunculin on the movement of nuclear components (e.g., herpes capsid; Forest *et al.*, 2005). Alternatively, latrunculin B may affect the polymerization of molecules other than actin (e.g., actin-related proteins).

In summary, we have shown that cleavage bodies frequently colocalize with DDX1 bodies and are found adjacent to gems and CBs during S phase. Our results suggest a general need for DDX1 bodies, CBs, and gems throughout interphase, consistent with a role (direct or indirect) in RNA transcription, splicing, or processing. CstF-64 in cleavage bodies may be preferentially required when DNA is replicated, perhaps for histone gene transcription, which is tightly coupled to DNA replication. The dramatic alteration in CPSF-100 and CstF-64 staining observed upon latrunculin B treatment suggests a role for actin polymerization or related processes in the transport of CPSF-100, CstF-64, and other proteins such as RNA polymerase II within the nucleus. Future work will involve further examination of the composition of the latrunculin-induced nuclear spicules and studying the role that nuclear actin plays in the transport of molecules associated with RNA metabolism.

REFERENCES

Andrade, L. E., Chan, E. K., Raska, I., Peebles, C. L., Roos, G., and Tan, E. M. (1991). Human autoantibody to a novel protein of the nuclear coiled body: immunological characterization and cDNA cloning of p80-coilin. J. Exp. Med. *173*, 1407–1419.

Andrade, L. E., Tan, E. M., and Chan, E. K. (1993). Immunocytochemical analysis of the coiled body in the cell cycle and during cell proliferation. Proc. Natl. Acad. Sci. USA *90*, 1947–1951.

Bettinger, B. T., Gilbert, D. M., and Amberg, D. C. (2004). Actin up in the nucleus. Nat. Rev. Mol. Cell. Biol. *5*, 410–415.

Bleoo, S., Sun, X., Hendzel, M. J., Rowe, J. M., Packer, M., and Godbout, R. (2001). Association of human DEAD box protein DDX1 with a cleavage stimulation factor involved in 3′-end processing of pre-MRNA. Mol. Biol. Cell *12*, 3046–3059.

Boisvert, F. M., Hendzel, M. J., and Bazett-Jones, D. P. (2000). Promyelocytic leukemia (PML) nuclear bodies are protein structures that do not accumulate RNA. J. Cell Biol. *148*, 283–292.

Bregman, D. B., Du, L., van der Zee, S., and Warren, S. L. (1995). Transcription-dependent redistribution of the large subunit of RNA polymerase II to discrete nuclear domains. J. Cell Biol. *129*, 287–298.

Burgers, P. M., and Bauer, G. A. (1988). DNA polymerase III from *Saccharomyces cerevisiae*. II. Inhibitor studies and comparison with DNA polymerases I and II. J. Biol. Chem. *263*, 925–930.

Callan, H. G., Gall, J. G., and Murphy, C. (1991). Histone genes are located at the sphere loci of *Xenopus* lampbrush chromosomes. Chromosoma *101*, 245–251.

Carmo-Fonseca, M., Pepperkok, R., Carvalho, M. T., and Lamond, A. I. (1992). Transcription-dependent colocalization of the U1, U2, U4/U6, and U5 snRNPs in coiled bodies. J. Cell Biol. *117*, 1–14.

Carvalho, T., Almeida, F., Calapez, A., Lafarga, M., Berciano, M. T., and Carmo-Fonseca, M. (1999). The spinal muscular atrophy disease gene product, SMN: a link between snRNP biogenesis and the Cajal (coiled) body. J. Cell Biol. *147*, 715–728.

Chen, H. C., Lin, W. C., Tsay, Y. G., Lee, S. C., and Chang, C. J. (2002). An RNA helicase, DDX1, interacting with poly(A) RNA and heterogeneous nuclear ribonucleoprotein K. J. Biol. Chem. *277*, 40403–40409.

Cioce, M. and Lamond, A. I. (2005). Cajal bodies: a long history of discovery. Annu. Rev. Cell Dev. Biol. *21*, 105–131.

Cooper, J. A. (1987). Effects of cytochalasin and phalloidin on actin. J. Cell Biol. *105*, 1473–1478.

Coue, M., Brenner, S. L., Spector, I., and Korn, E. D. (1987). Inhibition of actin polymerization by latrunculin A. FEBS Lett. *213*, 316–318.

Dellaire, G., and Bazett-Jones, D. P. (2004). PML nuclear bodies: dynamic sensors of DNA damage and cellular stress. Bioessays *26*, 963–977.

Ehrenberg, M., and McGrath, J. L. (2004). Actin motility: staying on track takes a little more effort. Curr. Biol. *14*, 931–932.

Eliceiri, G. L., and Ryerse, J. S. (1984). Detection of intranuclear clusters of Sm antigens with monoclonal anti-Sm antibodies by immunoelectron microscopy. J. Cell. Physiol. *121*, 449–451.

Fakan, S., Leser, G., and Martin, T. E. (1984). Ultrastructural distribution of nuclear ribonucleoproteins as visualized by immunocytochemistry on thin sections. J. Cell Biol. *98*, 358–363.

Forest, T., Barnard, S., and Baines, J. D. (2005). Active intranuclear movement of herpesvirus capsids. Nat. Cell Biol. *7*, 429–431.

Frey, M. R., and Matera, A. G. (1995). Coiled bodies contain U7 small nuclear RNA and associate with specific DNA sequences in interphase human cells. Proc. Natl. Acad. Sci. USA *92*, 5915–5919.

Gall, J. G. (2000). Cajal bodies: the first 100 years. Annu. Rev. Cell Dev. Biol. *16*, 273–300.

Gall, J. G., Bellini, M., Wu, Z., and Murphy, C. (1999). Assembly of the nuclear transcription and processing machinery: Cajal bodies (coiled bodies) and transcriptosomes. Mol. Biol. Cell *10*, 4385–4402.

Gall, J. G., Stephenson, E. C., Erba, H. P., Diaz, M. O., and Barsacchi-Pilone, G. (1981). Histone genes are located at the sphere loci of newt lampbrush chromosomes. Chromosoma *84*, 159–171.

Gedge, L. J., Morrison, E. E., Blair, G. E., and Walker, J. H. (2005). Nuclear actin is partially associated with Cajal bodies in human cells in culture and relocates to the nuclear periphery after infection of cells by adenovirus 5. Exp. Cell. Res. *303*, 229–239.

Grande, M. A., van der Kraan, I., van Steensel, B., Schul, W., de The, H., van der Voort, H. T., de Jong, L., and van Driel, R. (1996). PML-containing nuclear bodies: their spatial distribution in relation to other nuclear components. J. Cell. Biochem. *63*, 280–291.

Gubitz, A. K., Feng, W., and Dreyfuss, G. (2004). The SMN complex. Exp. Cell Res. *296*, 51–56.

Hebert, M. D., Shpargel, K. B., Ospina, J. K., Tucker, K. E., and Matera, A. G. (2002). Coilin methylation regulates nuclear body formation. Dev. Cell *3*, 329–337.

Hebert, M. D., Szymczyk, P. W., Shpargel, K. B., and Matera, A. G. (2001). Coilin forms the bridge between Cajal bodies and SMN, the spinal muscular atrophy protein. Genes Dev. *15*, 2720–2729.

Heintz, N., Sive, H. L., and Roeder, R. G. (1983). Regulation of human histone gene expression: kinetics of accumulation and changes in the rate of synthesis and in the half-lives of individual histone mRNAs during the HeLa cell cycle. Mol. Cell. Biol. *3*, 539–550.

Kanai, Y., Dohmae, N., and Hirokawa, N. (2004). Kinesin transports RNA: isolation and characterization of an RNA-transporting granule. Neuron *43*, 513–525.

Kiseleva, E., Drummond, S. P., Goldberg, M. W., Rutherford, S. A., Allen, T. D., and Wilson, K. L. (2004). Actin- and protein-4.1-containing filaments link nuclear pore complexes to subnuclear organelles in *Xenopus* oocyte nuclei. J. Cell Sci. *117*, 2481–2490.

Lamond, A. I., and Spector, D. L. (2003). Nuclear speckles: a model for nuclear organelles. Nat. Rev. Mol. Cell. Biol. *4*, 605–612.

Lefebvre, S. *et al.* (1995). Identification and characterization of a spinal muscular atrophy-determining gene. Cell *80*, 155–165.

Lerner, E. A., Lerner, M. R., Janeway, C. A., Jr., and Steitz, J. A. (1981). Monoclonal antibodies to nucleic acid-containing cellular constituents: probes for molecular biology and autoimmune disease. Proc. Natl. Acad. Sci. USA *78*, 2737–2741.

Liu, J., Hebert, M. D., Ye, Y., Templeton, D. J., Kung, H., and Matera, A. G. (2000). Cell cycle-dependent localization of the CDK2-cyclin E complex in Cajal (coiled) bodies. J. Cell Sci. *113*(Pt 9), 1543–1552.

Liu, Q., and Dreyfuss, G. (1996). A novel nuclear structure containing the survival of motor neurons protein. EMBO J. *15*, 3555–3565.

Ma, T., Van Tine, B. A., Wei, Y., Garrett, M. D., Nelson, D., Adams, P. D., Wang, J., Qin, J., Chow, L. T., and Harper, J. W. (2000). Cell cycle-regulated phosphorylation of p220(NPAT) by cyclin E/Cdk2 in Cajal bodies promotes histone gene transcription. Genes Dev. *14*, 2298–2313.

Martincic, K., Campbell, R., Edwalds-Gilbert, G., Souan, L., Lotze, M. T., and Milcarek, C. (1998). Increase in the 64-kDa subunit of the polyadenylation/cleavage stimulatory factor during the G0 to S phase transition. Proc. Natl. Acad. Sci. USA *95*, 11095–11100.

Matera, A. G. (1999). Nuclear bodies: multifaceted subdomains of the interchromatin space. Trends Cell Biol. *9*, 302–309.

Matera, A. G., and Frey, M. R. (1998). Coiled bodies and gems: Janus or gemini? Am. J. Hum. Genet. *63*, 317–321.

Nelson, D. M., Ye, X., Hall, C., Santos, H., Ma, T., Kao, G. D., Yen, T. J., Harper, J. W., and Adams, P. D. (2002). Coupling of DNA synthesis and histone synthesis in S phase independent of cyclin/cdk2 activity. Mol. Cell. Biol. *22*, 7459–7472.

Ogg, S. C., and Lamond, A. I. (2002). Cajal bodies and coilin—moving towards function. J. Cell Biol. *159*, 17–21.

Pederson, T., and Aebi, U. (2002). Actin in the nucleus: what form and what for? J. Struct. Biol. *140*, 3–9.

Pederson, T., and Robbins, E. (1971). A method for improving synchrony in the G2 phase of the cell cycle. J. Cell Biol. *49*, 942–945.

Pellizzoni, L., Baccon, J., Charroux, B., and Dreyfuss, G. (2001a). The survival of motor neurons (SMN) protein interacts with the snoRNP proteins fibrillarin and GAR1. Curr. Biol. *11*, 1079–1088.

Pellizzoni, L., Charroux, B., Rappsilber, J., Mann, M., and Dreyfuss, G. (2001b). A functional interaction between the survival motor neuron complex and RNA polymerase II. J. Cell Biol. *152*, 75–85.

Pellizzoni, L., Yong, J., and Dreyfuss, G. (2002). Essential role for the SMN complex in the specificity of snRNP assembly. Science *298*, 1775–1779.

Raska, I. (1995). Nuclear ultrastructures associated with the RNA synthesis and processing. J. Cell. Biochem. *59*, 11–26.

Raska, I., Andrade, L. E., Ochs, R. L., Chan, E. K., Chang, C. M., Roos, G., and Tan, E. M. (1991). Immunological and ultrastructural studies of the nuclear coiled body with autoimmune antibodies. Exp. Cell Res. *195*, 27–37.

Schul, W., Groenhout, B., Koberna, K., Takagaki, Y., Jenny, A., Manders, E. M., Raska, I., van Driel, R., and de Jong, L. (1996). The RNA 3′ cleavage factors CstF 64 kDa and CPSF-100 kDa are concentrated in nuclear domains closely associated with coiled bodies and newly synthesized RNA. EMBO J. *15*, 2883–2892.

Schul, W., van Der Kraan, I., Matera, A. G., van Driel, R., and de Jong, L. (1999). Nuclear domains enriched in RNA 3′-processing factors associate with coiled bodies and histone genes in a cell cycle-dependent manner. Mol. Biol. Cell *10*, 3815–3824.

Schul, W., van Driel, R., and de Jong, L. (1998). Coiled bodies and U2 snRNA genes adjacent to coiled bodies are enriched in factors required for snRNA transcription. Mol. Biol. Cell *9*, 1025–1036.

Spector, I., Shochet, N. R., Blasberger, D., and Kashman, Y. (1989). Latrunculins—novel marine macrolides that disrupt microfilament organization and affect cell growth: I. Comparison with cytochalasin D. Cell Motil. Cytoskelet. *13*, 127–144.

Thelander, L., and Reichard, P. (1979). Reduction of ribonucleotides. Annu. Rev. Biochem. *48*, 133–158.

Tucker, K. E., Berciano, M. T., Jacobs, E. Y., LePage, D. F., Shpargel, K. B., Rossire, J. J., Chan, E. K., Lafarga, M., Conlon, R. A., and Matera, A. G. (2001). Residual Cajal bodies in coilin knockout mice fail to recruit Sm snRNPs and SMN, the spinal muscular atrophy gene product. J. Cell Biol. *154*, 293–307.

Wu, C. H., and Gall, J. G. (1993). U7 small nuclear RNA in C snurposomes of the *Xenopus* germinal vesicle. Proc. Natl. Acad. Sci. USA *90*, 6257–6259.

Wu, C. H., Murphy, C., and Gall, J. G. (1996). The Sm binding site targets U7 snRNA to coiled bodies (spheres) of amphibian oocytes. RNA *2*, 811–823.

Wu, Z. A., Murphy, C., Callan, H. G., and Gall, J. G. (1991). Small nuclear ribonucleoproteins and heterogeneous nuclear ribonucleoproteins in the amphibian germinal vesicle: loops, spheres, and snurposomes. J. Cell Biol. *113*, 465–483.

Yang, L., Guan, T., and Gerace, L. (1997). Lamin-binding fragment of LAP2 inhibits increase in nuclear volume during the cell cycle and progression into S phase. J. Cell Biol. *139*, 1077–1087.

Yong, J., Pellizzoni, L., and Dreyfuss, G. (2002). Sequence-specific interaction of U1 snRNA with the SMN complex. EMBO J. *21*, 1188–1196.

Young, P. J., Le, T. T., thi Man, N., Burghes, A. H., and Morris, G. E. (2000). The relationship between SMN, the spinal muscular atrophy protein, and nuclear coiled bodies in differentiated tissues and cultured cells. Exp. Cell Res. *256*, 365–374.

Young, P. J., Le, T. T., Dunckley, M., Nguyen, T. M., Burghes, A. H., and Morris, E. (2001). Nuclear gems and Cajal (coiled) bodies in fetal tissues: nucleolar distribution of the spinal muscular atrophy protein, SMN. Exp. Cell Res. *265*, 252–261.